Journal of The Electrochemical Society, **160** (2) A279-A284 (2013)
0013-4651/2013/160(2)/A279/6/$28.00 © The Electrochemical Society

Improved Capacity Retention for $LiVO_2$ by Cr Substitution

Xiaohua Ma, Geoffroy Hautier, Anubhav Jain, Robert Doe, and Gerbrand Ceder*,z

Department of Materials Science and Engineering, Massachusetts Institute of Technology, Cambridge, Massachusetts 02139, USA

We present a layered Li-intercalation oxide that operates on the V^{3+}/V^{4+} redox couple. The stabilization effect of adding a +3 element into the layered $LiVO_2$ has been studied by first principles calculations. We identified Cr substitution into $LiVO_2$ to be promising for stabilizing a layered material based on the V redox couple. Layered $LiCr_xV_{1-x}O_2$ (x = 0.1, 0.2, 0.4, 0.5) has been synthesized and tested electrochemically. The improved capacity retention confirms that the structural stability of delithiated $LiVO_2$ is improved by Cr doping.
 [DOI: 10.1149/2.046302jes]

Manuscript submitted September 26, 2012; revised manuscript received November 16, 2012. Published December 5, 2012.

Layered materials with the R-3m layered structure and composition $LiMO_2$ (M = transition metals) have shown to be remarkably good as high energy density cathode materials for rechargeable batteries. $LiCoO_2$ [1] is the original Li intercalation material from which the rechargeable Li battery industry grew. $LiNiO_2$ [2,3] also has excellent Li cycling capability and Li mobility, but is not used in pure form due to its high oxidation character when delithiated. Among more recently developed cathode materials only those in the family of layered Li(Li, Ni, Co, Mn)O_2 have so far been able to offer improved energy density.[4–6] It is therefore of interest to understand the potential of other layered compounds, and, if they do not reversibly intercalate, what their failure mode is. The most common failure modes are decomposition by reduction from the electrolyte or transition metal migration. The latter, for example, results in a layered to spinel transformation in partially delithiated Li_xMnO_2.[7,8] Reed et al. has proposed a model to explain the mechanism of ion migration using first principles calculations,[8,9] and found that Mn could migrate to tetrahedral sites when trivacancies are formed in the Li layer. The energy barrier for the migration is merely 0.4 eV, making the migration very easy. Meanwhile, a Li ion can migrate to a tetrahedral site in the adjacent Li layer to form a Li/Mn dumbbell configuration. It is actually this Li/Mn dumbbell that stabilizes and promotes Mn migration.

Layered $LiVO_2$ shows similar behavior to layered $LiMnO_2$ when it is cycled as an electrode material.[7,10] When $LiVO_2$ is partially delithiated, V migrates into Li layers, destroying the layered structure,[11,12] and resulting in a negligible discharge capacity.[13] As $LiVO_2$ and $LiMnO_2$ share the same structure, it is likely that the V migration mechanism is similar to that of Mn migration in $LiMnO_2$. Previous attempts to stabilize $LiVO_2$ upon delithiation include synthesizing an off-stoichiometric $Li_{0.86}V_{0.8}O_2$ [14,15] or a solid solution of $LiVO_2$ and Li_2TiO_3.[13]

In this work, we attempt to stabilize the layered $LiVO_2$ by introducing inactive +3 elements into the V site. We were motivated to attempt this strategy based on a high-throughput battery design project[16,17] that systematically attempted metal substitutions into known compounds,[18] and identified several $LiVO_2 - LiMO_2$ mixtures as promising cathodes offering a good compromise between theoretical energy density and thermal stability in the charged state. In our calculations, we study the stability of different $LiM_{0.5}V_{0.5}O_2$ mixtures (with M = Cr, Ti, Ga, Al, Fe, Ni, Mn, Co) and show that Cr is among the most energetically favored elements to mix with V in the layered structure. We also computationally demonstrate that vanadium migration in $LiVO_2$ is easily achievable through the Li/V dumbbell mechanism,[9,19] and that this migration is prevented by the presence of chromium in $LiCr_{0.5}V_{0.5}O_2$. Finally, we confirm our computational finding by presenting experimental results on the $LiCr_xV_{1-x}O_2$ (x = 0.1, 0.2, 0.4, 0.5) layered compound, showing that the capacity retention improves significantly when the Cr content is above 20%. However, in situ XRD results show some partial structural transformation during charge and discharge.

Methods

Computational.— Computational results are derived from Density Functional Theory (DFT) calculations within the Generalized Gradient Approximation (GGA) using the Perdue-Burke-Ernzerhof (PBE) pseudo-potential as implemented in VASP.[20] A +U correction term in the Dudarev scheme was used for V, Cr, Mn, Fe, Co and Ni. The exact U values we used in this work were defined by Jain et al.[17] from fitting enthalpy of formation for binary oxides following the method by Wang et al.[21] All stability and voltage computations were performed using the aflow wrapper around VASP and the parameters proposed by Jain et al.[17,22]

Stability computations for the different $LiM_{0.5}V_{0.5}O_2$ mixtures (with M = Cr, Ti, Ga, Al, Fe, Ni, Mn, Co) were performed by choosing ten orderings of M and V using an enumeration algorithm proposed by Hart et al.[23] After DFT relaxation the total energy obtained for these mixtures was compared for stability at zero K to all known phases in the ICSD database as well as linear combinations of them using the convex hull construction. Computations obtained from GGA and GGA+U are mixed following the scheme proposed by Jain et al.[24] For each compound, the energy for decomposition to more stable products, or "energy above the hull", was evaluated. The energy above the hull is always non-negative. A large energy above the hull indicates a less stable compound. Stable phases at 0 K have an energy above the hull of 0 meV/at.

Voltages were computed using the method proposed by Aydinol et al.[25] The entropic contribution was neglected. For each $LiM_{0.5}V_{0.5}O_2$ mixture (with M = Cr, Ti, Ga, Al, Fe, Ni, Mn, Co), we computed the average voltage at half capacity and full capacity (removing half a Li per formula unit and one lithium). In the cases of half delithiation, the Li and vacancy ordering was chosen with the same method as for M and V ordering.[23]

Thermal stability of the delithiated states ($Li_{0.5}M_{0.5}V_{0.5}O_2$ and $M_{0.5}V_{0.5}O_2$) was studied using the method presented by Ong et al.[26,27] The critical oxygen chemical potential for oxygen gas evolution was computed. The oxygen chemical potential is referenced to be 0 in air at 298 K using the oxygen energy fitted by Wang et al.[28]

In the investigation of ion migration, a periodical supercell of 12 primitive $Li_{0.5}Cr_{0.5}V_{0.5}O_2$ or $Li_{0.5}VO_2$ unit cells was used as well as a plane-wave basis with a kinetic energy cutoff of 520 eV and a reciprocal-space k-point grid of 2×2×2. The activation energy barriers were calculated with selective dynamics, where the migrating ion at the unstable activation state is fixed relative to distant ions in the supercell so that it will not relax to the stable initial or end position during the structural relaxation. The ions surrounding the migrating ion, however, were allowed to freely relax.[29]

Experimental.— $LiCr_xV_{1-x}O_2$ (x = 0.1, 0.2, 0.4, 0.5) samples were synthesized by solid-state reactions. Stoichiometric amounts of

*Electrochemical Society Active Member.
zE-mail: gceder@mit.edu

Table I. Oxidation states, stability and voltages for various layered $LiM_{0.5}V_{0.5}O_2$.

M in $LiM_{0.5}V_{0.5}O_2$	Oxidation states	Energy above hull (meV/atom)	Voltage (V) $LiM_{0.5}V_{0.5}O_2 \rightarrow Li_{0.5}M_{0.5}V_{0.5}O_2$	Voltage (V) $Li_{0.5}M_{0.5}V_{0.5}O_2 \rightarrow M_{0.5}V_{0.5}O_2$
Ti	Ti^{4+}, V^{2+}	0	1.9	3.1
Cr	Cr^{3+}, V^{3+}	3	2.7	3.6
Ga	Ga^{3+}, V^{3+}	17	2.9	3.7
Al	Al^{3+}, V^{3+}	22	2.8	3.3
Fe	Fe^{3+}, V^{3+}	48	2.7	3.5
Ni	Ni^{2+}, V^{4+}	47	3.2	4.5
Mn	Mn^{2+}, V^{4+}	77	2.6	3.7
Co	Co^{2+}, V^{4+}	91	2.8	3.7

$LiOH \cdot H_2O$ (98%, Alfa Aesar), $Cr_3(OH)_2(CH_3COO)_7$ (Cr 24%, Alfa Aesar) and V_2O_5 (99.2%, Alfa Aesar) were mixed and ball milled in aceton for 12 hours at a rate of 300 rpm. The mixture slurry was dried into a powder, and about 0.5 g of powder was pressed into a pellet. The pellet was fired at 800°C in an argon flow for 12 hours before it was slowly cooled to room temperature.

Electrodes were fabricated using 60 wt% active material, 35 wt% super P carbon and 5 wt% PTFE as a binder, and tested in Swagelok cells using 1 M $LiPF_6$ in EC:DMC (1:1 in volume) as the electrolyte, and Li foil as the negative electrode. Swagelok cells were assembled in a glove box filled with argon, and galvanostatically charged and discharged at a rate of C/10 where 1C is theoretical capacity.

The in situ electrochemical cell consists of two aluminum plates measuring 4×4 cm^2. Each has an 8 mm diameter hole at the center, which is covered by a Beryllium disk. The cathode foil, separator and Li foil are placed between the Beryllium windows. A rubber gasket is placed between two Al plates for sealing. The in situ X-ray diffraction patterns were collected on the beam line X16C at the National Synchrotron Light Source of Brookhaven National Laboratory. The wavelength of the X-ray source was 0.7027 Å. The full transmission diffraction patterns was recorded within minutes by using a strip detector that consists of 640 channels spanning a total angle of 8.704°.

Results

Using DFT computations, we investigated the energies of substituting various elements M for V in the layered structure. Table I shows stability in the lithiated state, voltage for delithiation and oxidation states for M = Cr, Ti, Ga, Al, Fe, Ni, Mn, and Co in $LiM_{0.5}V_{0.5}O_2$. The stability at 0 K of the lithiated state is assessed by the convex hull construction. This procedure effectively compares the energy of a phase to all linear combination of competing phases, based on a database of calculated properties for all unique ICSD compounds.[17,30] The energy above the hull indicates how far from stability a phase is. A compound with zero energy above hull is stable at 0 K. Based on known DFT errors,[31] compounds with an energy above hull of under about 50 meV/atom also have a fair probability of being synthesizable. The table also indicates the oxidation state of vanadium and the element M. The oxidation states have been deduced from the magnetic moment present on the element at the completion of the DFT relaxation. Voltages for the first and second half of the capacity have also been computed.

According to the calculated results in Table I, the most stable mixture is between vanadium and Ti or Cr. However, Ti is oxidized to +4 while V is reduced to +2 when they are mixed. This is detrimental to the voltage that can be obtained from the material, as the first half of the capacity will correspond to the V^{2+}/V^{3+} couple, resulting in a very low voltage of 1.9 V. The gallium and aluminum alloys are not as stable as Ti and Cr mixtures but are still within the range of possible DFT errors[31] or within the range that can be stabilized by entropic factors. Moreover, the convex hull has been constructed using the 0 K ground state for $LiGaO_2$ and $LiAlO_2$ but at high temperature those two compounds are known to form layered structures. When the ground state structures are suppressed from the construction, we find that the $Li_{0.5}Ga_{0.5}V_{0.5}O_2$ and $Li_{0.5}Al_{0.5}V_{0.5}O_2$ are respectively only 6 meV/atom and 13 meV/atom above hull. This indicates that the two compounds are more favored energetically at high temperature. Considering its stability and voltage, we chose to investigate $LiCr_{0.5}V_{0.5}O_2$ although we suspect that Ga and Al substituted systems may also be synthesizable.

In $LiCr_{0.5}V_{0.5}O_2$, the average voltage at 2.7 V in the first half of the charge corresponds therefore to the V^{3+}/V^{4+} couple, while the 3.6 V voltage is associated with the V^{4+}/V^{5+} couple (Table I). The study of the calculated magnetic moments upon delithiation shows that Cr is inactive and stays +3. It is interesting to see that a similar capacity as for the pure $LiVO_2$ compound (296 mAh/g) is still achievable when half of the active transition metal is replaced by an inactive element. This is due to the potential for two electron extraction exhibited by V^{3+}. While delithiation of $LiVO_2$ up to one Li per formula unit activates the +3 to +4 couple, $LiCr_{0.5}V_{0.5}O_2$ can in principle also have one lithium per formula unit extracted by activating the +3 to +5 couple of V.

The large theoretical capacity available leads to attractive theoretical specific energy and energy density for $LiCr_{0.5}V_{0.5}O_2$ (940 Wh/kg and 3781 Wh/l). These attractive energy densities are combined with a good thermal stability of the delithiated state. The safety of charged cathode materials is currently of great concern and can be related to the tendency for a cathode material to release oxygen upon heating.[32,33] We recently developed a method to assess this tendency to release oxygen gas by computing the critical oxygen chemical potential for oxygen evolution. A high oxygen chemical potential will be associated with materials more easily releasing oxygen, and therefore more likely to be thermally unstable.[27] Fig. 1 shows the computed oxygen chemical potential of the delithiated $LiCr_{0.5}V_{0.5}O_2$ (in red) and compares it to a few known battery materials (in blue). In contrast to layered $LiCoO_2$, $LiCr_{0.5}V_{0.5}O_2$ is predicted to possess exceptional thermal stability. While the CoO_2 oxygen chemical potential is higher than 0 and therefore would thermodynamically release oxygen gas at 298 K in air, the vanadium based compound is closer to $FePO_4$, one of the most thermally stable cathode materials.[33–35]

Possible cation migration in layered $Li_{0.5}VO_2$ and $Li_{0.5}Cr_{0.5}V_{0.5}O_2$ was investigated by computing the energy along the migration path from the transition metal layer to a site in the Li layer. Fig. 2a shows

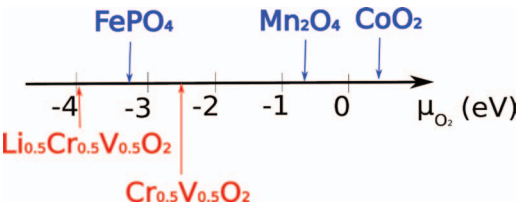

Figure 1. Critical oxygen chemical potentials for oxygen gas evolution for a few known charged cathodes (in blue) and for the half delithiated and fully delithiated $LiCr_{0.5}V_{0.5}O_2$ (in red).

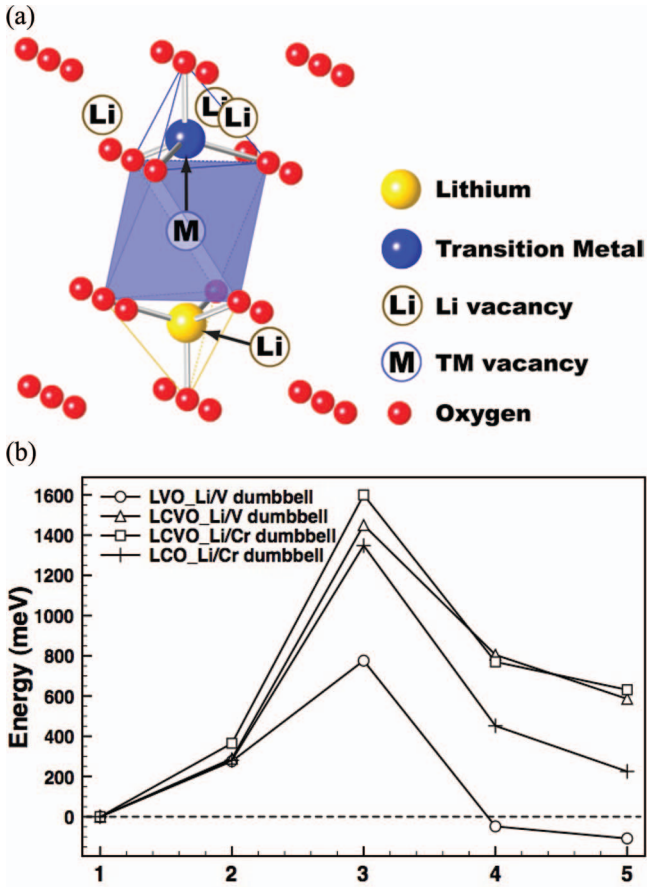

Figure 2. (a) Demonstration of the formation of Li/M dumbbell configuration through the migration of transition metal M and Li along the arrows; (b) Energies along the path of ion migration to form a Li/M dumbbell configuration. ◯ is for the Li/V dumbbell in $Li_{0.5}VO_2$; Δ for the Li/V dumbbell in $Li_{0.5}Cr_{0.5}V_{0.5}O_2$; □ for the Li/Cr dumbbell in $Li_{0.5}Cr_{0.5}V_{0.5}O_2$; + for the Li/Cr dumbbell in $Li_{0.5}CrO_2$. Along the path: 1) half delithiated layered structure with no transition metal in the Li layer; 2) Li disorder to create a trivacancy around a tetrahedron in the Li layer; 3) a single transition metal atom located at the energy saddle point in the hop between octahedron and tetrahedron; 4) a single transition metal atom in an Li layer tetrahedron; 5) Li/M dumbbell.[19]

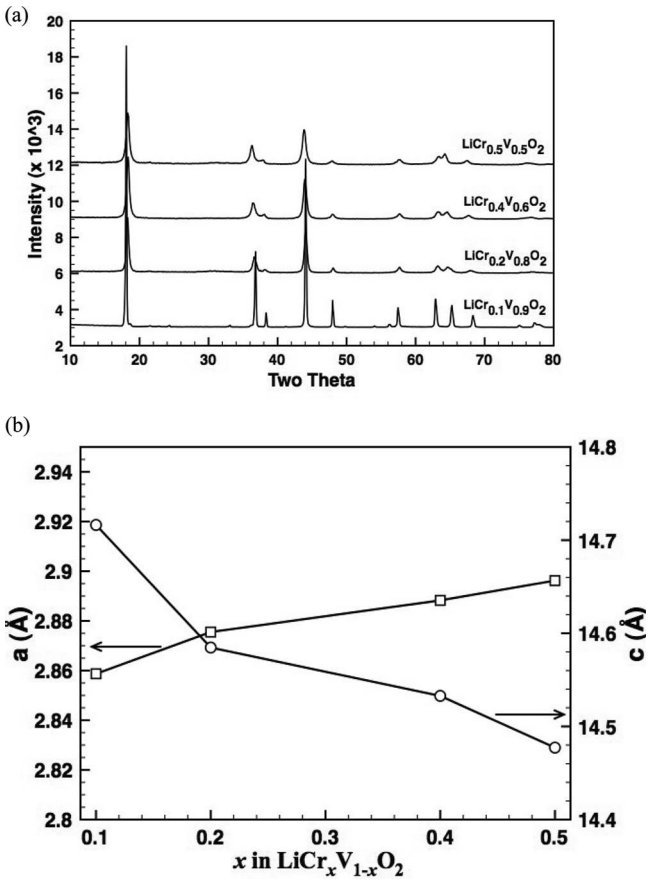

Figure 3. (a) X-ray diffraction patterns, and (b) lattice constants for $LiCr_xV_{1-x}O_2$ (x = 0.1, 0.2, 0.4, 0.5). Minor peaks of $LiCr_{0.1}V_{0.9}O_2$ in (a) might be from trace amount of impurities.

the formation of the Li/M dumbbell configuration. The first step in Li/M dumbell formation is the creation of a trivacancy in the Li layer, followed by migration of the M from the octahedral site into the face-sharing tetrahedral site in the Li layer. Meanwhile, one Li moves to the tetrahedral site on the other side of the now vacant M-site. The details of the formation of a Li/M dumbbell configuration can also be found in our previous papers.[9,19]

Fig. 2b compares the energy barriers of ion migration in half delithiated $LiVO_2$ and $LiCr_{0.5}V_{0.5}O_2$. Forming a Li/V dumbbell configuration in $Li_{0.5}VO_2$ lowers the energy by 0.11 eV, indicating that the Li/V dumbbell configuration is preferred thermodynamically. The energy barrier for the V migration is 0.78 eV. Previous work has shown energy barriers in partial delithiated $LiMnO_2$ (∼ 0.4 eV), $LiCoO_2$ (∼ 1.6 eV) and $LiNi_{2/3}Sb_{1/3}O_2$ (∼ 0.6 eV).[9,19] Experimental evidence demonstrates that $LiMnO_2$ and $LiNi_{2/3}Sb_{1/3}O_2$ will essentially transform into a spinel type structure,[7] while the layered structure of $LiCoO_2$ remains stable.[36,37] As the migration barrier in $LiVO_2$ is substantially closer to that in $LiMnO_2$ and $LiNi_{2/3}Sb_{1/3}O_2$, V migration in $Li_{0.5}VO_2$ via the dumbell mechanism is very likely to occur. In $Li_{0.5}Cr_{0.5}V_{0.5}O_2$, however, energies of both Li/V and Li/Cr dumbbell configurations are about 0.6 eV higher than that of the layered structure, and the energy barriers for both V and Cr migration are as high as ∼1.5 eV, very close to that of Co migration in $LiCoO_2$. With this high migration barrier, the migration of V or Cr is unlikely. Therefore, our first principles calculations indicate that Cr substitution inhibits ion migration in half delithiated $LiCr_xV_{1-x}O_2$ systems.

Inspired by the computational results, we synthesized $LiCr_xV_{1-x}O_2$ (x = 0.1, 0.2, 0.4, 0.5) by solid-state reactions. X-ray diffraction patterns in Fig. 3a show a single layered phase for the as-prepared $LiCr_xV_{1-x}O_2$ (x = 0.1, 0.2, 0.4, 0.5). Rietveld refinements with the space group R-3m give a good fit for all the four compounds. Lattice constants from the refinements are shown in Fig. 3b. The lattice constant a increases while c decreases with Cr doping, which is consistent with the results obtained by Goodenough et al.[38] The decrease of c parameter is expected with the substitution of a smaller Cr^{3+} ion (r_{Cr} = 0.615 Å) for a V^{3+} ion (r_V = 0.640 Å). The a parameter, however, anomalously increases with increasing Cr content. It is known that vanadium atoms within the V plane of $LiVO_2$ cluster to form V_3 trimers at room temperature.[39] This clustering shrinks the V-V distance, making the a parameter of $LiVO_2$ significantly smaller than that of $LiCrO_2$, even though the V^{3+} ion is larger than Cr^{3+}. Cr doping into the V plane increases the a parameter by prohibiting the formation of V_3 trimers.[38]

Fig. 4 shows galvanostatic charge and discharge profiles of $LiCr_xV_{1-x}O_2$ at C/10 at selected cycles., $LiCr_{0.1}V_{0.9}O_2$ shows a capacity of ∼120 mAh/g for the first charge at the plateau around 2.8 V which can be attributed to the V^{3+}/V^{4+} redox couple.[11] However, it delivers only a capacity of ∼30 mAh/g in the first discharge, and behaves similarly to $LiVO_2$.[13] In the following nine cycles, $LiCr_{0.1}V_{0.9}O_2$ largely retains its small capacity of ∼30 mAh/g. When the amount of Cr is increased to 20%, the V^{3+}/V^{4+} plateau is raised by ∼0.1 V in the first charge, and becomes more sloping. Meanwhile, an additional plateau around 4.1 V shows up, which is possibly attributed to the Cr^{3+}/Cr^{4+} redox couple as the average voltage of Cr^{3+}/Cr^{4+} couple in

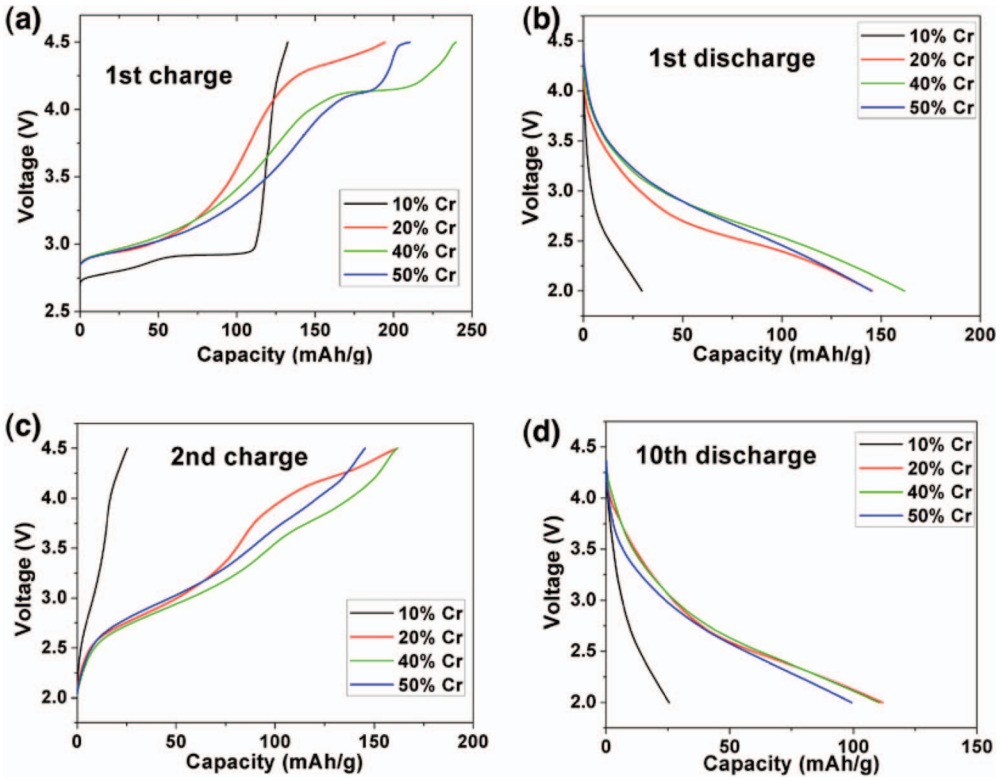

Figure 4. Galvanostatic charge and discharge of $LiCr_xV_{1-x}O_2$ ($x = 0.1, 0.2, 0.4, 0.5$) at a C/10 rate. (a) First charge to 4.5V; (b) First discharge to 2V; (c) Second charge; (d) 10th discharge.

layered $LiCrO_2$ was calculated to be about 4.11 V.[40] The first discharge of all samples with 20% or more Cr is significantly better than that of 10% Cr sample, with the discharge capacity reaching 150 mAh/g. For the second charge, $LiCr_{0.2}V_{0.8}O_2$ shows a capacity of 150 – 160 mAh/g, and the two plateaus around 2.8 V and 4.1 V become less distinct. After ten cycles, the discharge capacity of $LiCr_{0.2}V_{0.8}O_2$ drops to 115 mAh/g. When the Cr content increases up to 40% and 50%, the electrochemical behavior is very similar to that of $LiCr_{0.2}V_{0.8}O_2$.

Fig. 5a shows the full transmission XRD patterns for $LiCr_{0.5}V_{0.5}O_2$ at various stages of its first charge and discharge. 2θ has been converted to that for the wavelength of Cu Kα. The broad peaks and backgrounds are from cell components such as separators, carbon and binders, etc. The doublet peaks around 71° is from the (102) diffraction of Beryllium disks on two sides of the in situ cell. Most peaks from the active material $LiCr_{0.5}V_{0.5}O_2$ shift in angle during charge and discharge, and the (018) diffraction disappears or merges with the (110) diffraction as shown in Fig. 5c. Fig. 5b shows an additional peak that appears closely below the (003) diffraction during the charge process, and remains until the end of discharge.

Discussion

Our first principles calculations demonstrate that the partial substitution of V with Cr increases the V^{3+} migration barrier by 0.67 eV, and additionally makes Li/V dumbell formation thermodynamically unstable. To understand the effect of Cr on the migration barrier, we investigated the oxidation states along the migration paths[9] (shown in Table II). In $Li_{0.5}VO_2$, the migrating V is in a +3 oxidation state at all three positions (octahedral, octahedral/tetrahedral face, and tetrahedral). In $Li_{0.5}Cr_{0.5}V_{0.5}O_2$, however, all V have been oxidized to +4. When one V^{4+} migrates to the tetrahedral site, it reduces to V^{3+}. Meanwhile, one of its nearest neighboring V^{4+} is oxidized into V^{5+}. The charge disproportionation can be written as $2V^{4+}(oct) \rightarrow V^{3+}(tet) + V^{5+}(oct)$. It is known that V^{5+} is energetically more stable in tetrahedral[41] or trigonal bipyramidal[42] sites due to its electronic configuration and small ionic size. The creation of V^{5+} in an octahe-

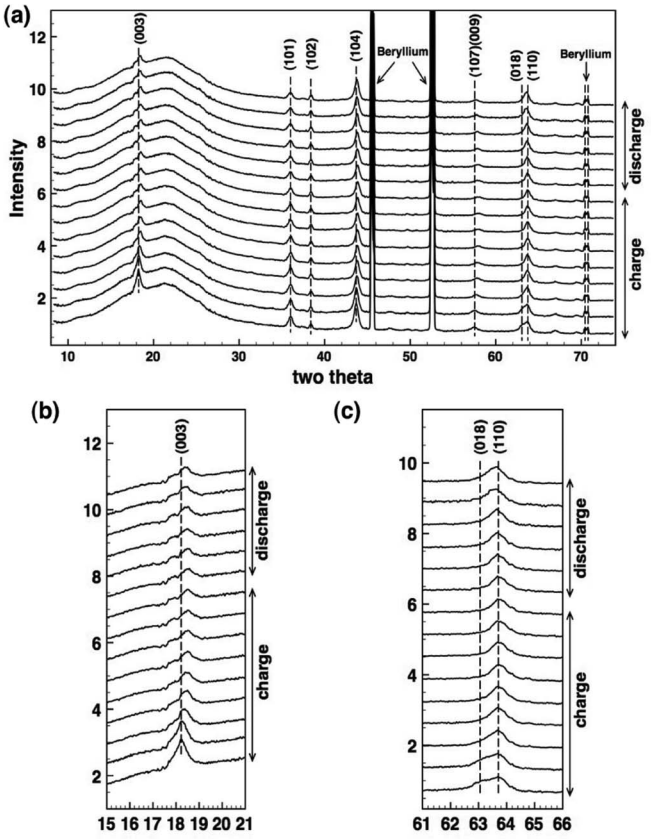

Figure 5. In-situ X-ray diffractions of $LiCr_{0.5}V_{0.5}O_2$ upon the first charge and discharge. (a) Full XRD patterns along the first charge and discharge; (b) (003) diffraction in a layered R-3m structure; (c) (018) and (110) diffractions. 2θ has been converted to that for the wavelength of Cu Kα.

Table II. Oxidation states of the migrating ions at different positions.

Migration ions	Octahedral oxidation state	Octa/Tetra face oxidation state	Tetrahedral oxidation state
V in $Li_{0.5}VO_2$	3	3	3
V in $Li_{0.5}Cr_{0.5}V_{0.5}O_2$	4	3	3
Cr in $Li_{0.5}Cr_{0.5}V_{0.5}O_2$	3	3	3
Cr in $Li_{0.5}CrO_2$	3	3.4	3.7

dral site by the reduction of the migration V^{4+}(oct) to V^{3+}(tet) may be what is responsible for the high migration barrier in $Li_{0.5}Cr_{0.5}V_{0.5}O_2$.

Our hypothesis based on oxidation state analysis suggests that V migration requires both a migrating V in the +3 oxidation state and Li trivancies. Before $LiCr_{0.5}V_{0.5}O_2$ is half delithiated, there are indeed V^{3+} available. However, significant V migration might not occur because a low concentration of Li vacancies in the early stage of the charge will result in very low concentration of trivacancies in the Li layer. When the Cr doping rate is very low (such as 10%), there are still significant amount of V^{3+} available when $LiCr_xV_{1-x}O_2$ is half delithiated. Thus, the V^{3+} can migrate into tetrahedral sites without forming V^{5+} in octahedral sites. To prevent octahedral V^{5+} formation to the point that it improves capacity, a higher amount of Cr doping, e.g. 20% or more, seems necessary. Hence, while V ions migrate isovalently as V^{3+} in Li_xVO_2, it is the oxidation enhanced migration of V in $Li_xCr_{0.5}V_{0.5}O_2$ that makes its migration more difficult.

The Cr migration barrier in $Li_{0.5}Cr_{0.5}V_{0.5}O_2$ is about 0.22 eV higher than in $Li_{0.5}CrO_2$, as is shown in Fig. 2b. In $Li_{0.5}CrO_2$, half the Cr are +3 and half are +4. The migrating Cr starts with a valence state of +3 but is oxidized to +3.7 on the migrating path as is shown in Table II. Meanwhile, one Cr^{4+} close to the migrating Cr ion obtains one electron, being reduced to Cr^{3+}. In $Li_{0.5}Cr_{0.5}V_{0.5}O_2$, however, all Cr stays in the +3 state during migration. The migration barrier of Cr in $Li_{0.5}Cr_{0.5}V_{0.5}O_2$ is about 0.22 eV higher than that in $Li_{0.5}CrO_2$, suggesting that Cr^{3+} is less mobile than Cr^{4+}. In $Li_{0.5}Cr_{0.5}V_{0.5}O_2$, however, the relatively more mobile Cr^{4+} cannot be formed through any possible charge disproportionation of V^{4+} and Cr^{3+}.

Our computational results indicate that V^{3+}(tet) is more stable than V^{4+}(tet), while Cr^{4+}(tet) is more stable than Cr^{3+}(tet), which is why Cr^{3+} needs to be oxidized while migrating, while V^{4+} needs to be reduced to migrate. This site preference can be explained based on the electronic states of the *3d* electrons. Fig. 6 shows schematically the relative position of *3d* states in the relevant sites.[41,43] When Cr^{4+} migrates from an octahedral (O_h) to a tetrahedral (T_d) site, two *3d* electrons are rearranged from t_{2g} orbitals of O_h to the *e* orbitals of T_d. As the two *e* orbitals are split off from the t_2 orbitals in the tetrahedral symmetry by a gap, Cr^{4+}(oct) is energetically preferred. With a similar analysis, it can be found that V^{3+}(tet) is energetically preferred while V^{4+}(tet) is not.

Although the measured capacity was significantly improved by substituting more than 20% Cr into $LiVO_2$, the in situ XRD results suggest that some structural change still occurs during charge and discharge. Fig. 5b shows one peak around 18° belonging to the (003) diffraction. During the charge process, the (003) diffraction shifts to higher angle indicating a decrease of the *c* lattice parameter. Meanwhile, an additional peak occurs below the (003) diffraction, which could be due to the (111) diffraction of a spinel-like structure.[44] In Fig. 5c, the adjacent (018) and (110) diffractions, which are defining characteristics of the layered structure, merge into one diffraction peak. It is possible that the two diffractions merge into one (440) diffraction of a spinel-like structure.[44,45] However, most other diffractions belonging to the layered structure, such as (003), have not changed significantly, implying that the structural transformation, if any, happens only partially. During the discharge process, the additional peak below the (003) diffraction remains, and the adjacent (018) and (110) diffractions are not recovered, indicating that the structural transformation is not reversible. However, results from first principles

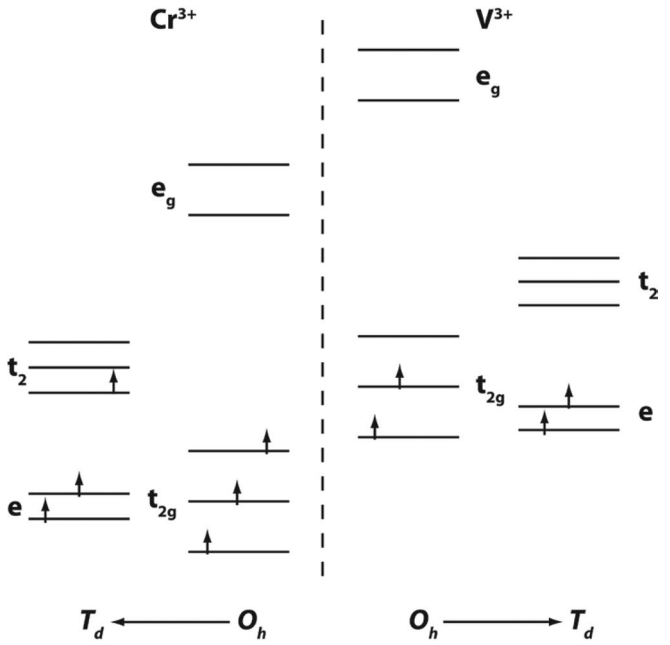

Figure 6. Schematic *3d* electron structures of Cr^{3+} and V^{3+} in octahedral (O_h) and tetrahedral (T_d) sites. The Cr^{4+}/V^{4+} is formed by removing the top electron of Cr^{3+}/V^{3+}.

calculations suggest that the structural transformation through the formation of Li/Cr or Li/V dumbbell configuration is unlikely at $x<0.5$ in $Li_xCr_{0.5}V_{0.5}O_2$. It is however possible that some V migration occurs for $x>0.5$ when V^{3+} is still present. While the trivacancy concentration will be smaller for $x>0.5$ it is nonetheless non-zero, and may lead to slow V^{3+} migration.

The 2.8 V plateau during first charge in Fig. 4a is very close to our calculated voltage of 2.7 V, which is attributed to the V^{3+}/V^{4+} redox couple. It also agrees with electrochemical results of layered $LiVO_2$.[13,14] The consistency between the calculated and experimental voltages also indicates that no structural transformation occurs during the early stage of the charge, which is consistent with the in situ XRD results. The 4.1 V plateau of $LiCr_xV_{1-x}O_2$ (x = 0.2, 0.4, 0.5) in Fig. 4a is about 0.5 V higher than the calculated V^{4+}/V^{5+} redox couple. The calculated 3.6 V for V^{4+}/V^{5+} assumes a perfect layered structure all through the charge process. The structural transformation shown in the in situ XRD may modify the V^{4+}/V^{5+} voltage. As is indicated by in situ XRD, spinel-like structures form partially with Li or V in the tetrahedral sites, which will block the Li diffusion paths significantly. It is possible that tetrahedral Li needs to be extracted before octahedral Li can be taken out, which could result in a higher voltage. We have tried to clarify the origin of the 4.1 V plateau by XPS analysis. However, the results turned out to be inconclusive due to the conjugation of oxidation state change and structural transformation.

Conclusions

First principles calculations indicated that Cr substitution into $LiVO_2$ can significantly increase the V migration barrier upon partial charge, and improve the structural stability with respect to Li/V dumbell formation. Electrochemical results of $LiCr_xV_{1-x}O_2$ show improved capacity, confirming the computational prediction. However, we still detect minor structural transformations that are yet to be fully understood. Further study of +3 metal doping into $LiVO_2$ might result in additional insights and better electrochemical performance.

Acknowledgment

This work was supported by the Robert Bosch Co. and by Umicore. The authors thank Dr. Hailong Chen and Prof. Peter Stephens for help with the in situ XRD.

References

1. K. Mizushima, P. C. Jones, P. J. Wiseman, and J. B. Goodenough, *Mat. Res. Bull.*, **15**, 783 (1980).
2. C. Delmas, J. P. Peres, A. Rougier, A. Demourgues, F. Weill, A. Chadwick, M. Broussely, F. Perton, P. Biensan, and P. Willimann, *J. Power Sources*, **68**, 120 (1997).
3. M. Broussely, F. Perton, P. Biensan, J. M. Bodet, J. Labat, A. Lecerf, C. Delmas, A. Rougier, and J. P. Peres, *J. Power Sources*, **54**, 109 (1995).
4. Y. Makimura and T. Ohzuku, *J. Power Sources*, **119-121**, 156 (2003).
5. N. Yabuuchi, Y. Koyama, N. Nakayama, and T. Ohzuku, *J. Electrochem. Soc.*, **152**, A1434 (2005).
6. K. Kang, Y. S. Meng, J. Breger, C. P. Grey, and G. Ceder, *Science*, **311**, 977 (2006).
7. Y. Shao-Horn, S. A. Hackney, A. R. Amstrong, P. G. Bruce, R. Gitzendanner, C. S. Johnson, and M. M. Thackeray, *J. Electrochem. Soc.*, **146**, 2404 (1999).
8. J. Reed, G. Ceder, and A. Van der Ven, *Electrochem. Solid-State Lett.*, **4**, A78 (2001).
9. J. Reed and G. Ceder, *Chem. Rev.*, **104**, 4513 (2004).
10. A. R. Armstrong and P. G. Bruce, *Nature*, **381**, 499 (1996).
11. L. A. Picciotto, M. M. Thackeray, and W. I. F. David, *Mat. Res. Bull.*, **19**, 1497 (1984).
12. M. Thackeray, L. A. Picciotto, W. I. F. David, P. G. Bruce, and J. B. Goodenough, *J. Solid State Chem.*, **67**, 285 (1987).
13. L. Zhang, K. Takada, N. Ohta, M. Osada, and T. Sasaki, *J. Power Sources*, **174**, 1007 (2007).
14. K. Ozawa, Y. Nakao, L. Wang, Z. Cheng, H. Fujii, M. Hase, and M. Eguchi, *J. Power Sources*, **174**, 469 (2007).
15. K. Ozawa, L. Wang, H. Fujii, M. Eguchi, M. Hase, and H. Yamaguchi, *J. Electrochem. Soc.*, **153**, A117 (2006).
16. G. Hautier, A. Jain, S. P. Ong, B. Kang, C. Moore, R. Doe, and G. Ceder, *Chem. Mater.*, **23**, 3495 (2011).
17. A. Jain, G. Hautier, C. J. Moore, S. P. Ong, C. C. Fischer, T. Mueller, K. A. Persson, and G. Ceder, *Comp. Mater. Sci.*, **50**, 2295 (2011).
18. G. Hautier, C. Fischer, V. Ehrlacher, A. Jain, and G. Ceder, *Inorg. Chem.*, **50**, 656 (2011).
19. X. Ma, K. Kang, G. Ceder, and Y. S. Meng, *J. Power Sources*, **173**, 550 (2007).
20. G. Kresse and J. Furthmüller, *Phys. Rev. B*, **54**, 11169 (1996).
21. L. Wang, T. Maxisch, and G. Ceder, *Phys. Rev. B*, **73**, 195107 (2006).
22. W. Setyawan and S. Curtarolo, *Comp. Mater. Sci.*, **49**, 299 (2010).
23. G. L. W. Hart and R. W. Forcade, *Phys. Rev. B*, **77**, 224115 (2008).
24. A. Jain, G. Hautier, S. Ong, C. Moore, C. Fischer, K. Persson, and G. Ceder, *Phys. Rev. B*, **84**, 045115 (2011).
25. M. K. Aydinol, A. F. Kohan, and G. Ceder, *J. Power Sources*, **68**, 664 (1997).
26. S. P. Ong, L. Wang, B. Kang, and G. Ceder, *Chem. Mater.*, **20**, 1798 (2008).
27. S. P. Ong, A. Jain, G. Hautier, B. Kang, and G. Ceder, *Electrochem. Comm.*, **12**, 427 (2010).
28. L. Wang, T. Maxisch, and G. Ceder, *Chem. Mater.*, **19**, 543 (2007).
29. J. S. Reed, Ph.D. Thesis "Ab-Initio Study of Cathode Materials for Lithium Batteries," pp. 278–279, MIT, USA, 2003.
30. www.materialsproject.org, (2010).
31. G. Hautier, S. P. Ong, A. Jain, C. J. Moore, and G. Ceder, *Phys. Rev. B*, **85**, 155208 (2012).
32. J. R. Dahn, E. W. Fuller, M. Obrovac, and U. von Sacken, *Solid State Ionics*, **69**, 265 (1994).
33. G. Chen and T. J. Richardson, *J. Power Sources*, **195**, 1221 (2010).
34. A. Yamada, S. C. Chung, and K. Hinokuma, *J. Electrochem. Soc.*, **148**, A224 (2001).
35. M. Takahashi, S. Tobishima, K. Takei, and Y. Sakurai, *Solid State Ionics*, **148**, 283 (2002).
36. H. Gabrisch, R. Yazami, and B. Fultz, *J. Power Sources*, **119-121**, 674 (2003).
37. H. Wang, Y.-I. Jang, B. Huang, D. R. Sadoway, and Y.-M. Chiang, *J. Electrochem. Soc.*, **146**, 473 (1999).
38. J. B. Goodenough, G. Dutta, and A. Manthiram, *Phys. Rev. B*, **43**, 10170 (1991).
39. P. F. Bongers, *Crystal Structure and Chemical Bonding in Inorganic Chemistry*, Chapter 4, Elsevier, New York, 1975.
40. S. Komaba, C. Takei, T. Nakayama, A. Ogata, and N. Yabuuchi, *Electrochem. Comm.*, **12**, 355 (2010).
41. J. B. Goodenough and A. L. Leob, *Phys. Rev.*, **98**, 391 (1955).
42. H. G. Bachmann, F. R. Ahmed, and W. H. Barnes, *Zeitschrift Für Kristallographic*, **115**, 110 (1961).
43. H. Bethe and R. Jackiw, *Intermediate Quantum Mechanics*, Addison Wesley Longman, Inc., Reading, MA, 1986.
44. S. Choi and A. Manthiram, *J. Electrochem. Soc.*, **149**, A1157 (2002).
45. G. Dutta, A. Manthiram, J. B. Goodenough, and J.-C. Grenier, *J. Solid State Chem.*, **96**, 123 (1992).